

https://doi.org/10.70917/jcc-2025-012 Article

Fabrication and Performance Analysis of Bi₂Te₃ and Sb₂Te₃ Thin Film Thermoelectric Generator for Waste Heat Recovery

Nurfarhana Ahmad Musri ^{1,*}, Yoganash Putthisigamany ¹, Puvaneswaran Chelvanathan ¹, Norasikin Ahmad Ludin ¹, Nadhrah Md Yatim ² and Ubaidah Syafiq ^{1,*}

- ¹ Solar Energy Research Institute (SERI), Universiti Kebangsaan Malaysia, Bangi 43600, Selangor, Malaysia; yoganashnash99@gmail.com (N.A.M.); cpuvaneswaran@ukm.edu.my (P.C.), sheekeen@ukm.edu.my (N.A.L.)
- Faculty of Science and Technology, Universiti Sains Islam Malaysia, Bandar Baru Nilai 71800, Negeri Sembilan, Malaysia; nadhrah@usim.edu.my
- * Corresponding author: farhanamusri@gmail.com (N.A.M.); ubaidahsyafiq@ukm.edu.my (U.S.)

Abstract: Hybridizing thermoelectric generators (TEGs) with renewable energy systems offers a promising route to enhance energy efficiency. However, conventional bulk TEG modules are bulky and impractical for applications requiring lightweight and flexible designs, such as building-integrated systems. This study addresses this limitation by developing a thin film TEG using stoichiometric bismuth telluride (Bi₂Te₃) and antimony telluride (Sb₂Te₃) deposited on a glass substrate via radio frequency magnetron sputtering. The structural, morphological, and thermoelectric properties of the films were analyzed using XRD, FESEM, EDX, Hall effect, and Seebeck coefficient measurements, confirming their suitability for device fabrication. The fabricated TEG, consisting of 6 n-type Bi₂Te₃ and p-type Sb₂Te₃ pairs, achieved a maximum open-circuit voltage of 208.55 mV and power output of 0.54 μW at a temperature difference of 125 K, with a maximum power per unit active planar area of 0.1 μW cm⁻². These results demonstrate the feasibility of thin film TEGs for integration into lightweight and compact energy-harvesting systems, highlighting their potential in renewable energy applications.

Keywords: thermoelectric generator (TEG); thin film; Bi₂Te₃; Sb₂Te₃; sputtering

1. Introduction

The global shift towards renewable energy is essential for achieving a sustainable, low-carbon future. However, as the deployment of renewable energy systems increases, so does the challenge of maximizing their efficiency due to fluctuating conditions. For instance, solar photovoltaic (PV) systems capture sunlight to generate electricity, yet only 5–20% of the sun rays are transformed into electricity while the remaining radiation is either transmitted backward or absorbed in the form of heat by the panel (Dwivedi et al., 2020). The heat absorbed by the panel increases its temperature causing irreversible degradation of its electric output power (Parthiban & Ponnambalam, 2022; Shaker et al., 2024). This waste heat can be repurposed and turned into valuable energy using an energy conversion device such as a thermoelectric generator (TEG), which can be integrated with the PV system to increase the overall power output. This integration enhances the overall power output of the system by generating additional electricity from the thermal energy. Instead of allowing the excess heat to dissipate, which could reduce PV efficiency, the TEGs transform it into a secondary energy source, improving the total system efficiency. Such hybrid systems are beneficial in applications where maximizing energy output is crucial, particularly in regions with high solar irradiance.

Thermoelectric (TE) materials have garnered significant attention in recent years due to their unique ability to directly convert heat into electrical energy via the Seebeck effect (Ochieng et al., 2022; Qasim



Copyright: © 2025 by the authors

et al., 2022). Given the current fast-growing demand for efficient energy conversion technologies, this feature makes them a promising solution for waste heat recovery and renewable energy applications. Among the various classes of TE materials, bismuth telluride (Bi₂Te₃) and antimony telluride (Sb₂Te₃) have emerged as frontrunners, owing to their exceptional TE properties at near-room temperatures (Pei et al., 2020; Soleimani et al., 2020). TE performance of a material is evaluated using the dimensionless figure of merit, $ZT = S^2 \sigma T/\kappa$. In this equation, S represents the Seebeck coefficient (V/K), σ denotes electrical conductivity (Ω .m⁻¹), κ indicates thermal conductivity (W/m.K), and T refers to the absolute temperature (K). For a TE material to have a good efficiency, it needs S and σ values to be as high as possible, and the κ value to be as low as possible.

The increasing interest in TE materials has led to a surge in research focused on enhancing their performance through various means, including nanostructuring (Bo et al., 2019; Jaldurgam et al., 2021; Kul'bachinskii, 2019) and alloying (Adam et al., 2020; Saberi & Sajjadi, 2022; Witting et al., 2020). Among the possible TEG configurations, thin film-based devices have shown considerable promise, including reduced thermal conductivity due to quantum confinement effects (Chen et al., 2020; Syafiq et al., 2022), better retention of the thermal gradient (Isram et al., 2023; Karthikeyan et al., 2020), and the potential for integration into micro- and nanoscale electronic devices (Yang et al., 2022; Zeng et al., 2020). Additionally, thin films enable the exploration of novel material combinations and structures that are not feasible in bulk form, potentially leading to enhanced TE performance. In particular, Bi₂Te₃ and Sb₂Te₃ have demonstrated remarkable potential to be fabricated as thin film TEG, with Bi₂Te₃ typically acting as an n-type semiconductor and Sb₂Te₃ as a p-type semiconductor (Musri et al., 2024; Vieira et al., 2019; Witting et al., 2019).

The performance of the TEG is heavily dependent on the quality of the thin films, which is influenced by factors such as film stoichiometry (Rogacheva et al., 2019; Sun et al., 2022), thickness (Andzane et al., 2021; Wanarattikan et al., 2019a), crystallinity (Amirghasemi & Kassegne, 2021; Z. hao Zheng et al., 2020), and the fabrication method used (Ma et al., 2021; Zhu et al., 2021). One of the primary challenges in the fabrication of Bi₂Te₃ and Sb₂Te₃ thin films is the precise control of film composition and thickness. Variation in stoichiometry can lead to significant changes in the electronic and thermal of the films, thereby affecting their overall thermoelectric performance (Kim et al., 2023). A study done by Yonezawa et al., 2020 shows that the carrier concentration of the film sample was significantly affected by the change in atomic composition, where Bi₂Te₃ changed to Bi₁Te₁ due to annealing. Their highest power factor was still less than that of well-established corresponding bulk alloys, due to the slightly deviated composition that included a certain number of defects such as vacancies and antisites caused by the evaporation of Te atoms. Therefore, the fabrication process must be carefully executed and optimized to produce high-quality, defect-free thin films for high-efficiency TEG.

This study aims to explore advanced deposition techniques for the fabrication of Bi_2Te_3 and Sb_2Te_3 thin films, followed by a comprehensive performance analysis of these films when integrated into a TEG. This work reports on the deposition and characterization of the Bi_2Te_3 and Sb_2Te_3 thin film on soda lime glass substrates along with performance analysis of the complete thin film TEG. The films were deposited via radio frequency (RF) magnetron sputtering technique with a top-down configuration, where the cathode was mounted at an angle to the substrate normal, leading to a more concentrated and convergent plasma to the substrate. By correlating the fabrication conditions with the resulting material properties and device performance, this research seeks to provide valuable insights into the fabrication of thin film TEGs in pursuit of a more sustainable energy generation.

1.1. Materials and Method

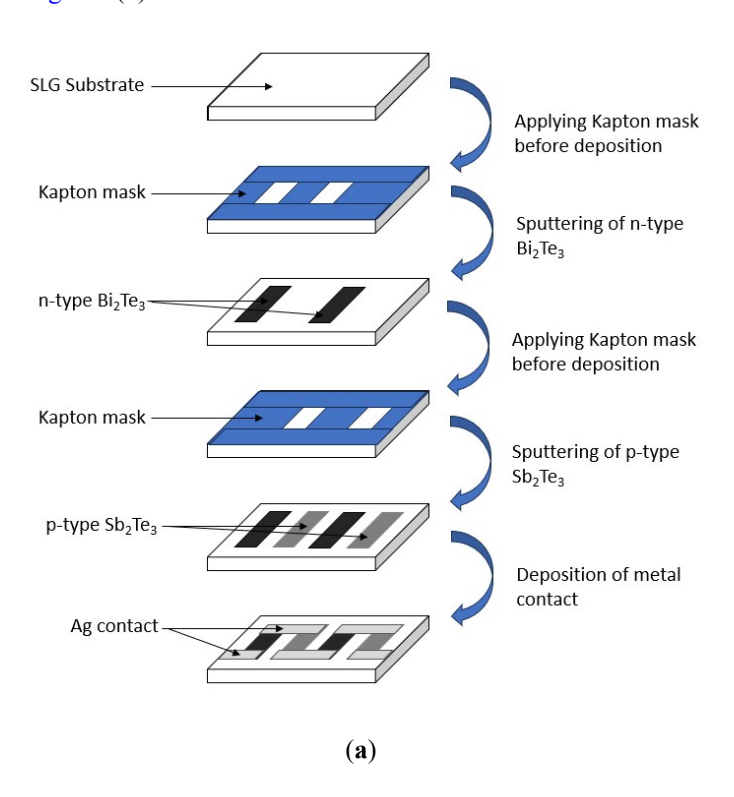
1.1.1. Deposition of Bi₂Te₃ and Sb₂Te₃ Thin Films

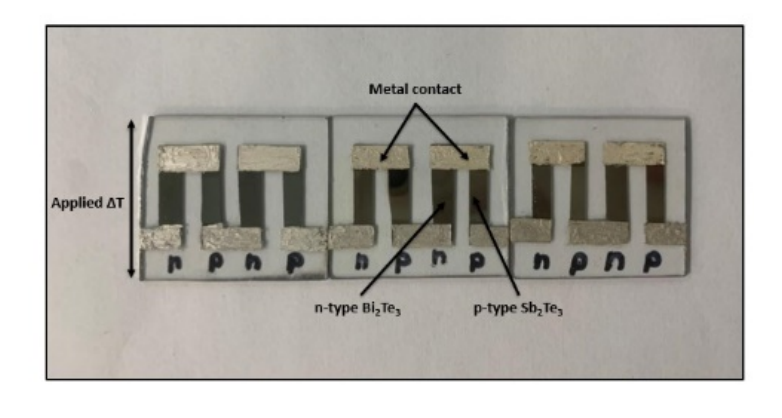
Bi₂Te₃ and Sb₂Te₃ thin films were deposited using RF magnetron sputtering on soda lime glass (SLG) substrates that were ultrasonically cleaned with methanol, acetone, ethanol, and deionized water for 10 mins to effectively remove organic contaminants and particulates. Nitrogen gas, hot plate, and UV ozone cleaner were also used to eliminate residues from the substrates. UV ozone treatment further eliminates residual hydrocarbons and introduces surface oxygen functional groups, enhancing surface energy and promoting strong interfacial bonding (Zhang et al., 2019). A sputter target of Bi₂Te₃ (diameter 50.8 mm, thickness 4.25 mm, 99.999% purity), Sb₂Te₃ (diameter 50.8 mm, thickness 6.35 mm, 99.999% purity), with argon gas (99.99% purity) were used for the sputter coating. The samples were deposited without substrate heating using RF power of 75 W for Bi₂Te₃ and 30 W for Sb₂Te₃ at the same deposition time of 60 mins. The parameters were chosen based on the optimised parameters obtained from our previous work (Musri et al., 2024) where the details of the deposition protocol were also extensively discussed. Different RF powers were used to compensate for variations in sputtering yield, atomic mass, and target density, ensuring comparable deposition rates and maintaining film stoichiometry.

The phase formation of the thin films was analyzed using an X'pert-pro PANalytical X-ray diffractometer with Cu K α radiation (λ = 1.5406 Å). The lattice parameters a and c were derived from Rietveld refinement of the experimental X-ray diffraction (XRD) data obtained from the as-deposited thin films. Structural reference files for Bi₂Te₃ (PDF 00-015-0863) and Sb₂Te₃ (PDF 01-071-0393) served as input data. Surface microstructure and film thickness were evaluated through topographic and cross-sectional images obtained by Field Emission Scanning Electron Microscopy (FESEM/JEOL, JSM7800F, operating at 3.0 kV). The film composition was confirmed via energy dispersive X-ray spectroscopy (EDX) attached to the FESEM. Hall voltage measurements were conducted using HMS ECOPIA 3000 with a fixed magnetic field of 0.57 T and probe currents of 10 mA and 0.8 mA for Bi₂Te₃ and Sb₂Te₃, respectively, to determine carrier concentration and conductivity. The Seebeck coefficient was measured in-plane using a Linseis LSR-3, with rectangular samples (about 2 cm × 1.25 cm) mounted for measurement. The absolute Seebeck coefficient was determined in a two-contact configuration relative to a Pt standard, applying a temperature gradient of approximately 25 °C.

1.1.2. Fabrication of Bi₂Te₃/Sb₂Te₃ Thin Film TEG

The thin film TEG was fabricated according to an illustration made by Isotta et al., 2022 with a few adjustments as shown in Figure 1(a). Clean rectangular SLG substrate were used to deposit the TE legs. Kapton mask was applied on the substrate leaving only the space required for sputtering n-type Bi₂Te₃, then Bi₂Te₃ was sputtered on the exposed area. The old Kapton mask was removed and a new one was applied to cover the n-type legs, using paper strips to protect the legs, leaving the area for p-type Sb₂Te₃. After that, Sb₂Te₃ was sputtered and when the mask was removed, the legs were in alternating positioned as shown in Figure 1(a). Finally, Ag paint was utilized to connect all legs in series due to its fast-drying properties and durability, which is crucial for preventing scratches during measurement. Unlike sputtered metal contacts, which may require additional adhesion layers and careful deposition control, Ag paint provides a simple, efficient, and low-contact-resistance solution that adheres well to thermoelectric materials. While contact resistance could influence overall performance, Ag paint forms a sufficiently conductive interface, ensuring stable electrical connections without significantly limiting the efficiency of the TEG. A schematic of the end TEG is visible in Figure 1(a) and the picture of the final thin film TEG is presented in Figure 1(b).



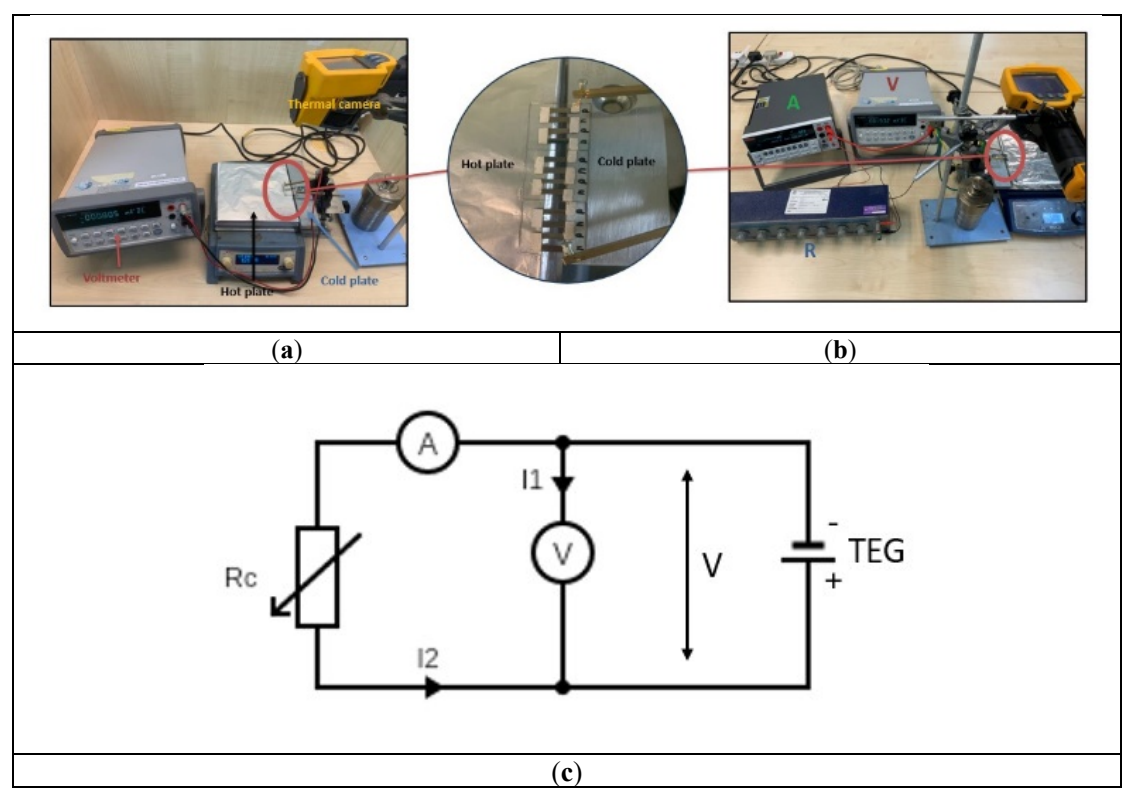


(b)

Figure 1. (a) Illustration of the steps to fabricate Bi₂Te₃/Sb₂Te₃ thin film TEG. (b) A scheme of the end thin film TEGs.

1.1.3. Performance Analysis of Bi₂Te₃/Sb₂Te₃ Thin Film TEG

All performance measurements were conducted under ambient conditions. Open-circuit voltage (Voc) as a function of temperature difference (ΔT) was recorded using a custom setup shown in Figure 2(a). A metal plate served as the heat sink (without active cooling), while a hot plate in contact with the bottom-lateral side of the TEG substrate acted as the heat source. At both ends of the TEG, contacts with springs were affixed, and a Keithley Agilent 34401A voltmeter was used to assess the voltage produced. The temperature of the hot plate was adjusted in increments of 10 °C, ranging from 70 °C to 250 °C. Temperature differences were monitored using a Fluke Ti₃₂ thermal camera, as illustrated in Figure 2(a) and Figure 2(b). Current–voltage–power (IVP) characteristics were measured using the setup arranged as shown in the I-V-P schematic in Figure 2(c), with the experimental setup depicted in Figure 2(b). For these measurements, a Keithley Agilent 34401A was used as the voltmeter, a FLUKE 8846A as the ammeter, and a variable resistor. The hot plate temperature was held constant at 250 °C. By recording I-V values across varying resistances, the power curve of the TEG was derived and plotted using P = VI.



177

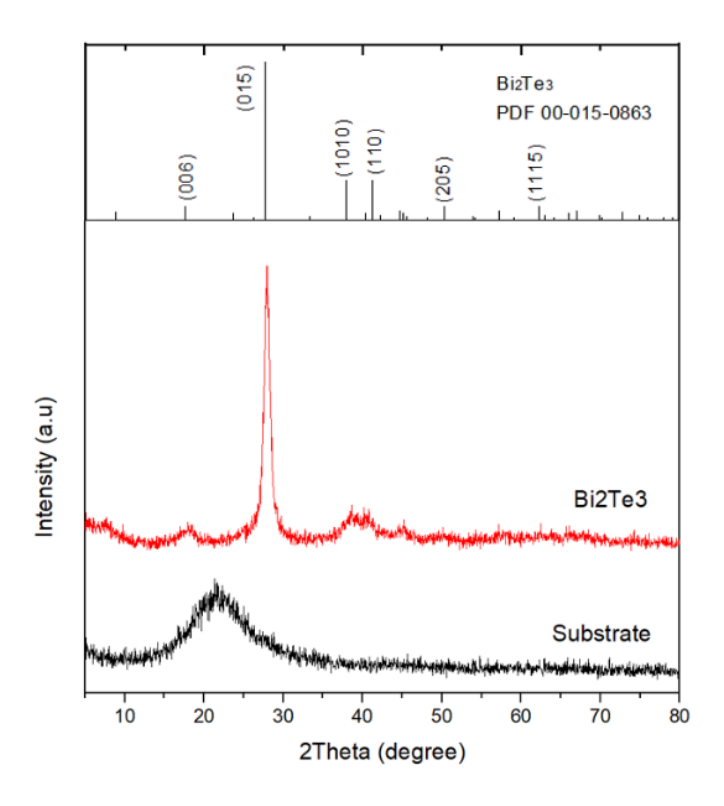
Figure 2. (a) In-house measuring setup for the V_{oc} versus ΔT plot. (b) In-house measuring setup for the I-V-P measurement. (c) Schematic of the setup connection used to measure the I-V-P characteristics.

2. Results and Discussion

2.1. Structural and Compositional Characterization of the Thin Films

The phase purity and crystallinity of the thin films were measured using X-ray diffraction (XRD) technique. As visible in Figure 3(a),(b) the XRD measurements indicate a good phase purity for both Bi_2Te_3 and Sb_2Te_3 samples, with no measurable trace of secondary phases. The XRD reflections observed for the Bi_2Te_3 and Sb_2Te_3 samples can be indexed with the respective rhombohedral Bi_2Te_3 phase (PDF # 00-015-0863) and Sb_2Te_3 phase (PDF # 01-071-0393) in the space group R-3m (166) with lattice parameters a = 4.3852 Å, c = 30.4830 Å for Bi_2Te_3 and a = 4.2640 Å, c = 30.4580 Å for Sb_2Te_3 . For the Bi_2Te_3 film, the observed reflections illustrate preferential growth along the c-axis with a sharp dominant peak growing anisotropically along the (0 1 5) direction, indicating a highly crystalline structure with a few small peaks corresponding to (0 0 6), (1 0 10) and (1 1 0) directions. For the Sb_2Te_3 film, a small and broad peak corresponding to the (0 1 5) direction due to the low thickness of the film, as proven by the FESEM cross-section image to be discussed. Overall, both XRD patterns do not show any peaks for secondary phases.

The FESEM micrograph shows that the as-deposited Bi_2Te_3 and Sb_2Te_3 films covers the entirety of the substrate in a continuous and homogenous manner. As can be seen in Figure 4(a),(d), Bi_2Te_3 films comprise of hexagonal grains, conforming the crystal structure of Bi_2Te_3 . The grains are densely packed with varying sizes, indicating a polycrystalline nature. The surface of the Sb_2Te_3 film exhibits more fine, rounded grains and is consistent in size compared to Bi_2Te_3 film, indicating a nearly amorphous phase resulting in a low and broad peak in XRD. From the cross-sectional view in Figure 4(b),(e), the interface between the film and the substrate looks distinct, with no significant diffusion between the two, suggesting good adhesion properties. From these images, the thickness of the films was estimated, yielding values of around $1.429 \pm 0.01~\mu m$ for Bi_2Te_3 thin films and $0.424 \pm 0.01~\mu m$ for Sb_2Te_3 thin films. Energy-dispersive X-ray spectroscopy (EDXS) was used to analyze the chemical composition of the films. The composition of the films was calculated from the EDXS spectra in Figure 4(c),(f), giving atomic percent of 41.9% Bi:58.1% Te, 40.0% Sb:60.0% Te. The estimated values show that both films gave a consistent Bi:Te and Sb:Te ratio of 2:3, indicating stoichiometric Bi_2Te_3 and Sb_2Te_3 were successfully fabricated.



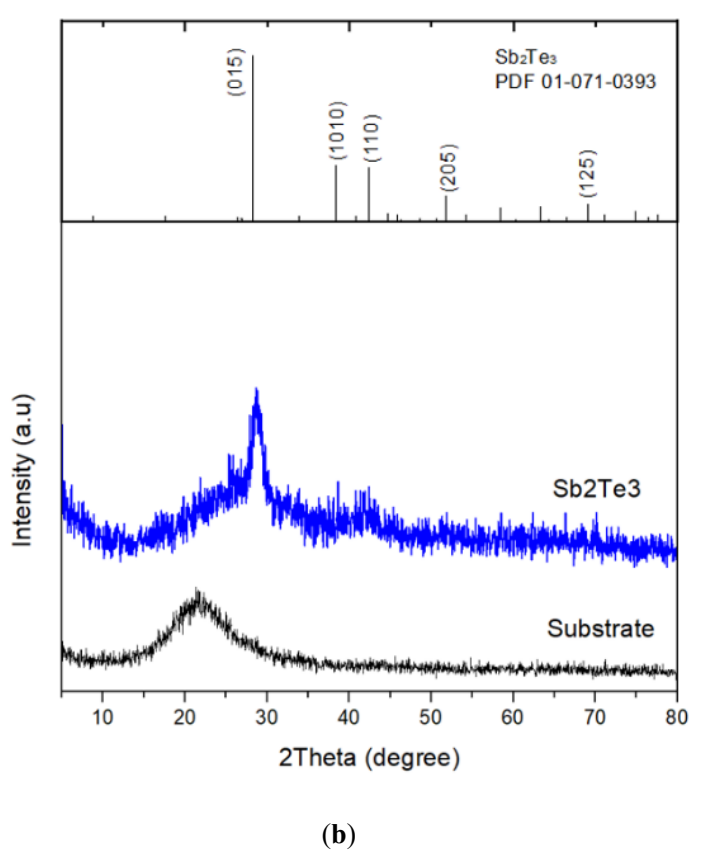


Figure 3. (a) XRD pattern of Bi₂Te₃ thin film. (b) XRD pattern of Sb₂Te₃ thin film.

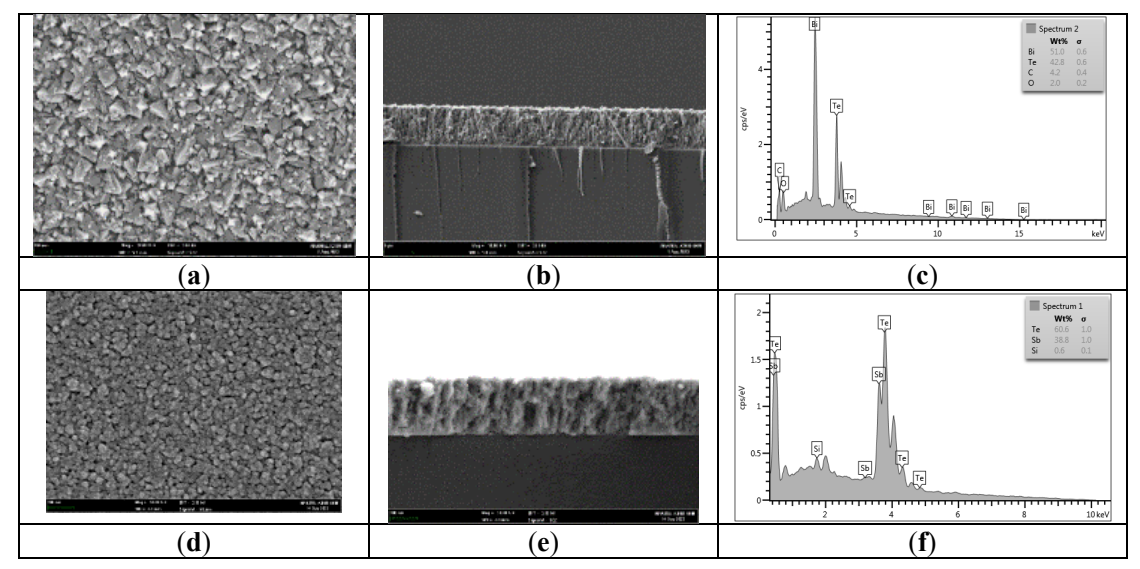


Figure 4. (a,b) FESEM surface and cross-section image of Bi₂Te₃ thin film. (c) EDXS spectra of Bi₂Te₃ thin film. (d,e) FESEM surface and cross-section image of Sb₂Te₃ thin film. (f) EDXS spectra of Sb₂Te₃ thin film.

2.2. Thermoelectric Characterization of the Thin Films

The Seebeck coefficients of the Bi_2Te_3 and Sb_2Te_3 thin films are reported in Figure 5, as a function of temperature in the range of 50-250 °C. The S values for Bi_2Te_3 are negative over the entire temperature range, but shown as an absolute value in the plot, highlighting its n-type behavior. Initially, the S value reached $-72.84 \,\mu\text{V/K}$ recorded at $\sim 50 \,$ °C. As the temperature increases, the S value gradually becomes more negative, reaching nearly $-200 \,\mu\text{V/K}$ at $\sim 200 \,$ °C. This trend suggests that the thermoelectric performance of Bi_2Te_3 is likely to increase as the temperature rises, which may be attributed to the

annealing effect where grain size and grain boundaries are improved (Zhao et al., 2021), consequently reducing the scattering effect (Zang et al., 2023). In contrast, Sb₂Te₃ displays a positive S across the temperature range, signifying p-type behavior. Starting at 336.11 μ V/K at ~50 °C, the S value decreases slightly as the temperature increases, falling to approximately 220 μ V/K at ~200 °C. This gradual decline suggests a relatively stable thermoelectric performance for Sb₂Te₃, although the slight decrease indicates some temperature dependence, possibly due to phase changes in the material (Y. Zheng et al., 2024). The contrasting behaviors of Bi₂Te₃ and Sb₂Te₃ emphasize their suitability for different thermoelectric applications. The measured S aligns with previously reported values for sputtered thin films, where S values for Bi₂Te₃ were in the range of 50–90 μ V/K, while Sb₂Te₃ in the range of 190–300 μ V/K (Junlabhut et al., 2020; Naumochkin et al., 2022; Wanarattikan et al., 2019b). The trends observed where S remains high and relatively stable suggest better performance at elevated temperatures. This information is essential for the development of thermoelectric devices tailored for particular temperature settings, ensuring optimal energy conversion efficiency.

Table 1 summarized the values of thermoelectric properties recorded at relative ambient temperature. The carrier concentration of the thin films measured using Hall effect measurement exhibits a negative value for Bi_2Te_3 , further confirming the n-type conductivity, and a positive value for Sb_2Te_3 , confirming the p-type conductivity. The electrical conductivity of the thin films was determined to calculate the power factor (*PF*) of each film. *PF* becomes a decisive parameter for the selection of thin film materials due to its configuration. A low thermal conductivity is ideal for good efficiency, however, the substrate typically dominates thermal transport in thin film configurations because of the significant difference in thickness (Isotta et al., 2022). The calculated *PF* was 0.5781 and 0.3451 μ W/K² cm for Bi_2Te_3 and Sb_2Te_3 thin films, respectively, which were quite low in comparison with other reported values (Tang et al., 2022). The *S* and σ values greatly influenced the *PF* of thermoelectric materials, calculated by $PF = S2\sigma$. However, these two properties exhibit an inverse relationship due to their mutual dependence on carrier concentration, where an increase in one promotes a decrease in the other (Musah et al., 2021).

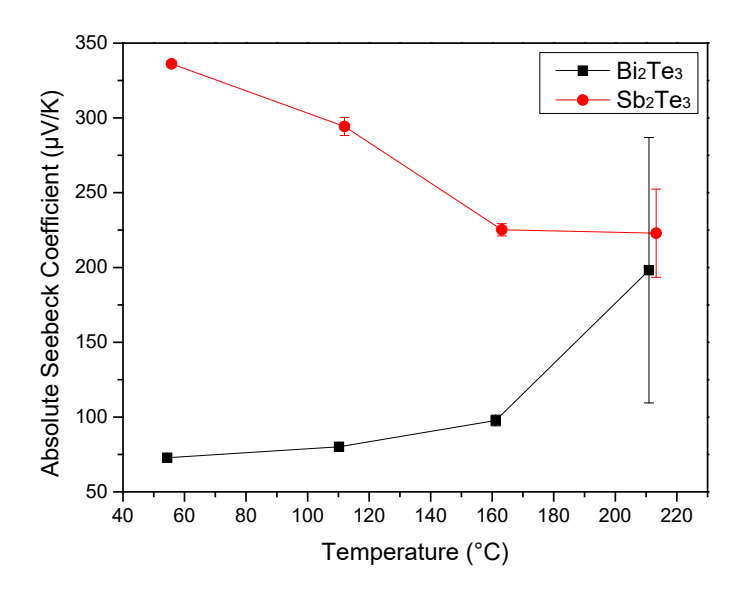


Figure 5. Absolute Seebeck coefficient, S of both Bi₂Te₃ and Sb₂Te₃ films.

Table 1. TE properties of both Bi₂Te₃ and Sb₂Te₃ thin film samples.

Target	RF power, (W)	Thickness (±0.01 μm)	Absolute Seebeck coefficient, S $(\mu V K^{-1})$	Carrier concentration, Nb (cm ⁻³)	Conductivity, $\sigma (\Omega \text{ cm})^{-1}$	Power Factor, PF (µW/K ² cm)
Bi ₂ Te ₃	75	1.429	-72.84	-5.71×10^{20}	108.96	0.5781
Sb ₂ Te ₃	30	0.424	336.11	1.44×10^{21}	6.05	0.3451

The trade-off between the S and σ in the films is evident from the results in Table 1. Sb₂Te₃ exhibits a significantly high S (336.11 μ V/K) but suffers from low σ (6.05 Ω^{-1} cm⁻¹), while Bi₂Te₃ has a lower S

 $(-72.84 \mu V/K)$ but a much higher σ (108.96 Ω^{-1} cm⁻¹). This inverse relationship arises due to carrier concentration differences, where Sb₂Te₃ has a higher Nb (1.44 × 10²¹ cm⁻³) compared to Bi₂Te₃ (-5.71 × 10²⁰ cm⁻³), leading to strong phonon scattering that reduces charge carrier mobility and, consequently, conductivity. The observed differences can be understood using the Boltzmann transport equation and the Mott relation (Kumar et al., 2021):

$$S = \frac{\pi^2 k^2_B T}{3e} \frac{1}{\sigma} \frac{d\sigma(E)}{dE} \bigg|_{E=E_F}$$
 (1)

This equation shows that S is inversely related to Nb; when Nb is high, more charge carriers are available for conduction, increasing σ but lowering S. Although a high S benefits thermoelectric voltage generation, the low σ in Sb₂Te₃ results in a reduced power factor ($PF = 0.3451 \,\mu\text{W/K}^2\text{cm}$), compared to $0.5781 \,\mu\text{W/K}^2\text{cm}$ for Bi₂Te₃. This highlights the well-known optimization challenge in thermoelectrics, where increasing carrier concentration can improve σ but typically degrades S, requiring careful doping and nanostructuring strategies to achieve an optimal balance for high efficiency.

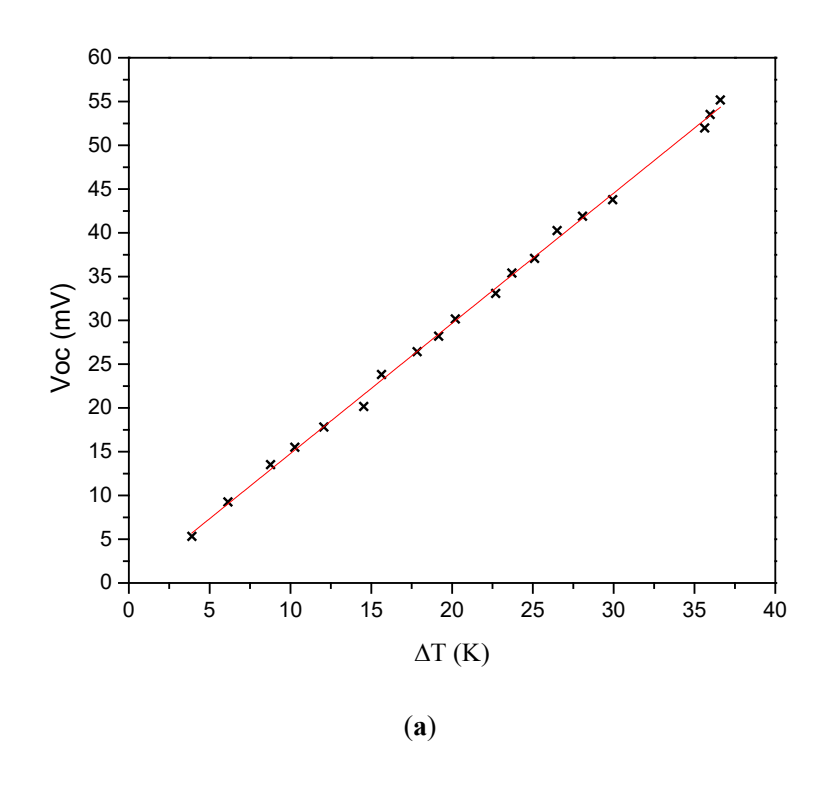
2.3. Performance Analysis of Bi₂Te₃/Sb₂Te₃ Thin Film TEG

Plotting the open circuit voltage (V_{oc}) against temperature differential (ΔT) is an essential tool for evaluating the performance of the TEG. This relationship helps to comprehend how effectively, in different thermal circumstances, a TEG can convert thermal energy into electrical energy. V_{oc} in a TEG is the voltage measured across the terminals of the device when no external load is connected, meaning no current flows through the circuit, and is directly proportional to both the S and ΔT (Al Qubeissi et al., 2020). This measurement also gives information on the maximum voltage that can be generated by the Bi₂Te₃/Sb₂Te₃ thin film TEG at specific ΔTs. The measurement was done in the temperature range of 70-250 °C, with a 10 °C increment. A metal plate served as the heat sink, and a hotplate was adjusted to raise the temperature of the hot side while maintaining the cold side at room temperature. However, due to poor heat sink setup and heat dispersion on the hotplate, the measured ΔTs did not fully match the set temperature of Th and Tc. The metal plate may accumulate heat over time, reducing the ΔT across the thermoelectric legs. To mitigate these issues, active cooling methods, such as fan-assisted or liquid cooling, can enhance heat extraction and maintain a stable ΔT. Figure 6(a) shows that the V_{oc} presents a linear trend of voltage with increasing applied temperature difference, depicting the ideal behavior of TEG (Li et al., 2020). The steep slope indicates high S, meaning the material of the TEG is effective at generating voltage from a given ΔT. The TEG with 6 pairs generated a maximum output voltage of 55 mV at ΔT 38 K.

Figure 6(b) shows the current-voltage IV and the current power IP curve of the Bi₂Te₃/Sb₂Te₃ thin film TEG. The IV curve represents the voltage as a function of current. The voltage starts at a maximum value when the current is zero, which corresponds to the open circuit voltage. As the current increases, the voltage decreases linearly, indicating that the internal resistance of the device dictates this behavior. The linear decline suggests Ohmic behavior, where the voltage drop is directly proportional to the current flowing through the device (Buchalik et al., 2021). On the other hand, The IP curve exhibits the classical parabolic shape. As the current begins to increase from zero, the power increases because both the current and the voltage contribute positively to the power output. However, as the current continues to increase, the voltage starts to drop significantly due to the internal resistance, leading to a decrease in power. The peak of the curve represents the maximum power point, where the product of current and voltage is maximized. This occurs when the load resistance matches the internal resistance of the device (Al Qubeissi et al., 2020). At this point, the power transferred to the load is at its maximum, and any further increase in current will cause the power to drop due to the decreasing voltage. The Bi₂Te₃/Sb₂Te₃ thin film TEG produces an impressive maximum power of 0.54 μW at 0.005 mA with ΔT 127 °C, meaning operating the TEG too far from this point (either at very high or very low currents) leads to suboptimal performance, as indicated by the declining power on either side of the peak. The maximum power per unit active planar area was calculated by dividing the maximum power with the area and number of TE legs, giving the value of $0.1 \,\mu\text{W cm}^{-2}$.

The measured power output achieved in this study is low compared to commercial bulk Bi₂Te₃-based TEGs, which typically achieve W/cm²-level power densities under similar temperature gradients (Maksymuk et al., 2022; Xu et al., 2022). This gap is primarily due to the intrinsic material differences between thin film and bulk thermoelectric materials. Bulk Bi₂Te₃ modules generally have higher carrier mobility and optimized doping, leading to superior electrical conductivity and power factor. Despite the lower power output, the thin film TEG in this study offer advantages such as flexibility, scalability, and integration into microelectronic devices, deposited with well-established industrial process suitable for real-world applications. Further optimization, such as improving film thickness, carrier concentration

tuning, and advanced thermal engineering, could help bridge the performance gap between thin-film and bulk TEGs.



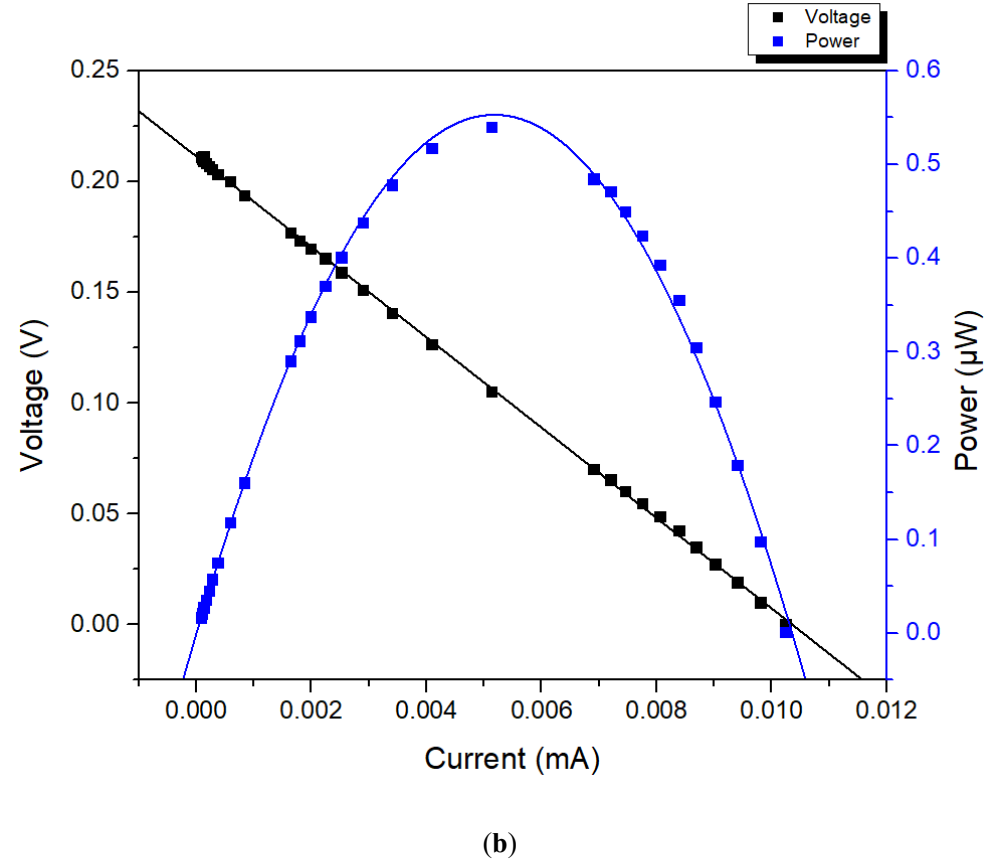


Figure 6. (a) V_{oc} versus ΔT of the Bi_2Te_3/Sb_2Te_3 thin film TEG. (b) I-V-P curves of the Bi_2Te_3/Sb_2Te_3 thin film TEG.

reported devices. The high ΔT (127 K) in this study results in a relatively high output voltage (211.6 mV), demonstrating strong thermoelectric response. The present Bi₂Te₃/Sb₂Te₃ thin-film TEG achieves an output voltage and power that are on par with (or exceed) several comparable devices in the literature, even with a modest number of p–n pairs and relatively compact dimensions. These results indicate that the fabrication approach is effective in producing a thin-film TEG capable of delivering strong performance at moderate temperature differences.

Table 2. Comparison of the performance data of the Bi₂Te₃/Sb₂Te₃ thin film TEG fabricated in the present work with those of devices published in the literature.

Reference, year	TE units	Device Dimension	ΔT (K)	Output Voltage (mV)	Output Power (µW)
this work, 2025	n-type Bi ₂ Te ₃ p-type Sb ₂ Te ₃	6 pairs; 3 mm × 15 mm × 1.429 μm n-type legs 3 mm × 15 mm × 0.424 μm p-type legs	127	211.6	0.54
Song et.al., 2024	n-type Bi ₂ Te ₃ p-type Bi _{0.5} Sb _{1.5} Te ₃	15 pairs; 2 mm × 2 mm × 400 nm	11	54.6	0.69
Chang et.al., 2020	$\begin{array}{c} \text{n-type} \\ \text{Bi}_2\text{Se}_{0.32}\text{Te}_{2.7} \\ \text{p-type} \\ \text{Bi}_{0.5}\text{Sb}_{1.5}\text{Te}_3 \end{array}$	3 pairs; 3.4 mm × 20 mm × 0.04 mm	54.9	~80	50.0
Kobayashi et.al., 2020	n-type Bi ₂ Te ₃ p-type Sb ₂ Te ₃	16 pairs; 130 mm × 20 mm × 125 μm	20	122.9	0.31
Viera et.al., 2019	n-type Bi ₂ Te ₃ p-type Sb ₂ Te ₃	15 pairs; 1 mm × 8 mm × 400 nm	35	210	0.70
Kong et.al., 2019	n-type Bi ₂ Te ₃	13 pairs	24	48.9	0.69
Takayama & Takashiri, 2017	n-type Bi ₂ Te ₃ p-type Sb ₂ Te ₃	11 pairs	28	32	0.15
Yang et.al., 2017	n-type Bi ₂ Te ₃ p-type Sb ₂ Te ₃	20 pairs; 0.3 mm × 6 mm × 400 nm	30	190	~0.15

3. Conclusion

In conclusion, the fabrication and performance analysis of Bi_2Te_3 and Sb_2Te_3 thin film TEG represent a significant advancement in the field of energy conversion technologies. Through careful fabrication technique, this study has demonstrated the potential of Bi_2Te_3 and Sb_2Te_3 thin film to achieve high thermoelectric efficiency. A prototype of thin film TEG with 6 pairs of Bi_2Te_3/Sb_2Te_3 legs was designed and fabricated, that able to achieve an impressive maximum power of 0.54 μ W at ΔT 127 °C. The calculated maximum power per unit active planar area obtained for the TEG was 0.1 μ W cm⁻². The ability to control film composition, thickness, and crystallinity is crucial in enhancing the electrical and thermal properties of these materials. Further optimization of the deposition parameters, film properties, and TEG structure needs to be studied to fully exploit the benefit of thin film configuration. The continued exploration of thin-film thermoelectrics, as exemplified by this study, holds the promise of making significant strides toward more efficient and practical applications of thermoelectric technology in the global quest for energy sustainability.

Authors' contributions

N. A. Musri: Conceptualization, methodology, formal analysis, writing—original draft, U. Syafiq.; supervision, resources, project administration, writing—review and editing, Y. Putthisigamany, P. Chelvanathan, N. A. Ludin, N. M Yatim; writing—review and editing, project administration, validation. All authors have read and agreed to the published version of the manuscript.

Funding

This research was funded by Universiti Kebangsaan Malaysia research grant: UKM-GGPM-2022-069.

Conflict of Interest Statement

The author(s) has/have no competing interests to declare.

References

- Adam, A. M., El-Khouly, A., Novitskii, A. P., Ibrahim, E. M. M., Kalugina, A. V., Pankratova, D. S., Taranova, A. I., Sakr, A. A., Trukhanov, A. V., Salem, M. M., & Khovaylo, V. (2020). Enhanced thermoelectric figure of merit in Bi-containing Sb2Te3 bulk crystalline alloys. *Journal of Physics and Chemistry of Solids*, 138. https://doi.org/10.1016/j.jpcs.2019.109262
- Al Qubeissi, M., El-Kharouf, A., & Soyhan, H. S. (n.d.). Renewable Energy-Resources, Challenges and Applications. Amirghasemi, F., & Kassegne, S. (2021). Effects of RF Magnetron Sputtering Deposition Power on Crystallinity and Thermoelectric Properties of Antimony Telluride and Bismuth Telluride Thin Films on Flexible Substrates. Journal of Electronic Materials, 50(4), 2190–2198. https://doi.org/10.1007/s11664-020-08681-y
- Andzane, J., Felsharuk, A., Sarakovskis, A., Malinovskis, U., Kauranens, E., Bechelany, M., Niherysh, K. A., Komissarov, I. V., & Erts, D. (2021). Thickness-dependent properties of ultrathin bismuth and antimony chalcogenide films formed by physical vapor deposition and their application in thermoelectric generators. Materials Today Energy, 19. https://doi.org/10.1016/j.mtener.2020.100587
- Bo, X., Tang, A., Dou, M., Li, Z., & Wang, F. (2019). Controllable electrodeposition and mechanism research of nanostructured Bi2Te3 thin films with high thermoelectric properties. *Applied Surface Science*, 486, 65–71. https://doi.org/10.1016/j.apsusc.2019.04.194
- Buchalik, R., Nowak, G., & Nowak, I. (2021). Mathematical model of a thermoelectric system based on steady- and rapid-state measurements. *Applied Energy*, 293. https://doi.org/10.1016/j.apenergy.2021.116943
- Chen, X., Zhou, Z., Lin, Y. H., & Nan, C. (2020). Thermoelectric thin films: Promising strategies and related mechanism on boosting energy conversion performance. In *Journal of Materiomics* (Vol. 6, Issue 3, pp. 494–512). Chinese Ceramic Society. https://doi.org/10.1016/j.jmat.2020.02.008
- Dwivedi, P., Sudhakar, K., Soni, A., Solomin, E., & Kirpichnikova, I. (2020). Advanced cooling techniques of P.V. modules: A state of art. Case Studies in Thermal Engineering, 21, 100674. https://doi.org/10.1016/j.csite.2020.100674
- Isotta, E., Andrade-Arvizu, J., Syafiq, U., Jiménez-Arguijo, A., Navarro-Güell, A., Gue, M., Saucedo, E., & Scardi, P. (2022). Towards Low Cost and Sustainable Thin Film Thermoelectric Devices Based on Quaternary Chalcogenides. Advanced Functional Materials, 32(32). https://doi.org/10.1002/adfm.202202157
- Isram, M., Magrin Maffei, R., Demontis, V., Martini, L., Forti, S., Coletti, C., Bellani, V., Mescola, A., Paolicelli, G., Rota, A., Benedetti, S., Bona, A. di, Ribeiro, J. M., Tavares, C. J., & Rossella, F. (2023). Thermoelectric and Structural Properties of Sputtered AZO Thin Films with Varying Al Doping Ratios. *Coatings*, 13(4). https://doi.org/10.3390/coatings13040691
- Jaldurgam, F. F., Ahmad, Z., & Touati, F. (2021). Synthesis and performance of large-scale cost-effective environment-friendly nanostructured thermoelectric materials. In *Nanomaterials* (Vol. 11, Issue 5). MDPI AG. https://doi.org/10.3390/nano11051091
- Junlabhut, P., Nuthongkum, P., Sakulkalavek, A., Harnwunggmoung, A., Limsuwan, P., & Sakdanuphab, R. (2020). Enhancing the thermoelectric properties of sputtered Sb2Te3 thick films via post-annealing treatment. Surface and Coatings Technology, 387. https://doi.org/10.1016/j.surfcoat.2020.125510
- Karthikeyan, V., Surjadi, J. U., Wong, J. C. K., Kannan, V., Lam, K. H., Chen, X., Lu, Y., & Roy, V. A. L. (2020). Wearable and flexible thin film thermoelectric module for multi-scale energy harvesting. *Journal of Power Sources*, 455(March), 227983. https://doi.org/10.1016/j.jpowsour.2020.227983
- Kim, S., Lee, Y. S., & Kim, N. H. (2023). Homogeneity- and Stoichiometry-Induced Electrical and Optical Properties of Cu-Se Thin Films by RF Sputtering Power. *Materials*, 16(18). https://doi.org/10.3390/ma16186087
- Kul'bachinskii, V. A. (2019). Nanostructuring and Creation of Nanocomposites as a Promising Way to Increase Thermoelectric Efficiency. *Nanotechnologies in Russia*, 14(7–8), 334–345. https://doi.org/10.1134/S1995078019040098
- Kumar, A., Bano, S., Govind, B., Bhardwaj, A., Bhatt, K., & Misra, D. K. (2021). A Review on Fundamentals, Design and Optimization to High ZT of Thermoelectric Materials for Application to Thermoelectric Technology. In *Journal of Electronic Materials* (Vol. 50, Issue 11, pp. 6037–6059). Springer. https://doi.org/10.1007/s11664-021-09153-7
- Li, K., Garrison, G., Moore, M., Zhu, Y., Liu, C., Horne, R., & Petty, S. (2020). An expandable thermoelectric power generator and the experimental studies on power output. *International Journal of Heat and Mass Transfer*, 160. https://doi.org/10.1016/j.ijheatmasstransfer.2020.120205

- Ma, Z., Wei, J., Song, P., Zhang, M., Yang, L., Ma, J., Liu, W., Yang, F., & Wang, X. (2021). Review of experimental approaches for improving zT of thermoelectric materials. In *Materials Science in Semiconductor Processing* (Vol. 121). Elsevier Ltd. https://doi.org/10.1016/j.mssp.2020.105303
- Maksymuk, M., Dzundza, B., Matkivsky, O., Horichok, I., Shneck, R., & Dashevsky, Z. (2022). Development of the high performance thermoelectric unicouple based on Bi2Te3 compounds. *Journal of Power Sources*, 530, 231301. https://doi.org/10.1016/j.jpowsour.2022.231301
- Musah, J. D., Ilyas, A. M., Novitskii, A., Serhiienko, I., Egbo, K. O., Saianand, G., Khovaylo, V., Kwofie, S., Yu, K. M., & Roy, V. A. L. (2021). Effective decoupling of seebeck coefficient and the electrical conductivity through isovalent substitution of erbium in bismuth selenide thermoelectric material. *Journal of Alloys and Compounds*, 857. https://doi.org/10.1016/j.jallcom.2020.157559
- Musri, N. A., Putthisigamany, Y., Chelvanathan, P., Ahmad Ludin, N., Md Yatim, N., & Syafiq, U. (2024). Fabrication of Bi2Te3 and Sb2Te3 Thermoelectric Thin Films using Radio Frequency Magnetron Sputtering Technique. *Journal of Visualized Experiments*, 2024(207). https://doi.org/10.3791/66248
- Naumochkin, M., Park, G. H., Nielsch, K., & Reith, H. (2022). Study of the Annealing Effects of Sputtered Bi2Te3
 Thin Films with Full Thermoelectric Figure of Merit Characterization. *Physica Status Solidi Rapid Research Letters*, 16(4). https://doi.org/10.1002/pssr.202100533
- Ochieng, A. O., Megahed, T. F., Ookawara, S., & Hassan, H. (2022). Comprehensive review in waste heat recovery in different thermal energy-consuming processes using thermoelectric generators for electrical power generation. *Process Safety and Environmental Protection*, 162, 134–154. https://doi.org/10.1016/j.psep.2022.03.070
- Parthiban, R., & Ponnambalam, P. (2022). An Enhancement of the Solar Panel Efficiency: A Comprehensive Review. In Frontiers in Energy Research (Vol. 10). Frontiers Media S.A. https://doi.org/10.3389/fenrg.2022.937155
- Pei, J., Cai, B., Zhuang, H. L., & Li, J. F. (2020). Bi2Te3-based applied thermoelectric materials: Research advances and new challenges. In *National Science Review* (Vol. 7, Issue 12, pp. 1856–1858). Oxford University Press. https://doi.org/10.1093/nsr/nwaa259
- Qasim, M. A., Velkin, V. I., & Hassan, A. K. (2022). Seebeck Generators and Their Performance in Generating Electricity. *Journal of Operation and Automation in Power Engineering*, 10(3), 200–205. https://doi.org/10.22098/joape.2022.9715.1677
- Rogacheva, E. I., Novak, K. V., Doroshenko, A. N., Nashchekina, O. N., & Budnik, A. V. (2019). Effect of deviation from stoichiometry on thermoelectric properties of Bi2Te3 polycrystals and thin films in the temperature range 77-300 K. *Journal of Nano- and Electronic Physics*, 11(5). https://doi.org/10.21272/jnep.11(5).05027
- Saberi, Y., & Sajjadi, S. A. (2022). A comprehensive review on the effects of doping process on the thermoelectric properties of Bi2Te3 based alloys. In *Journal of Alloys and Compounds* (Vol. 904). Elsevier Ltd. https://doi.org/10.1016/j.jallcom.2022.163918
- Shaker, L. M., Al-Amiery, A. A., Hanoon, M. M., Al-Azzawi, W. K., & Kadhum, A. A. H. (2024). Examining the influence of thermal effects on solar cells: a comprehensive review. *Sustainable Energy Research*, 11(1). https://doi.org/10.1186/s40807-024-00100-8
- Soleimani, Ž., Zoras, S., Ceranic, B., Shahzad, S., & Cui, Y. (2020). A review on recent developments of thermoelectric materials for room-temperature applications. *Sustainable Energy Technologies and Assessments*, 37. https://doi.org/10.1016/j.seta.2019.100604
- Sun, Z.-W., Cheng, K.-W., Lin, S.-W., Ranganayakulu, V. K., Chen, Y.-Y., Chiu, S.-J., Lee, T.-W., & Wu, A. T. (2022). Stoichiometric Effect of Sb ₂ Te ₃ Thin Film on Thermoelectric Property. *ACS Applied Energy Materials*, 5(6), 7026–7033. https://doi.org/10.1021/acsaem.2c00657
- Syafiq, U., Isotta, E., Ataollahi, N., Lohani, K., Luong, S., Trifiletti, V., Fenwick, O., & Scardi, P. (2022). Facile and Low-Cost Fabrication of Cu/Zn/Sn-Based Ternary and Quaternary Chalcogenides Thermoelectric Generators. ACS Applied Energy Materials, 5(5), 5909–5918. https://doi.org/10.1021/acsaem.2c00268
- Tang, X., Li, Z., Liu, W., Zhang, Q., & Uher, C. (2022). A comprehensive review on Bi 2 Te 3 -based thin films: Thermoelectrics and beyond . *Interdisciplinary Materials*, *I*(1), 88–115. https://doi.org/10.1002/idm2.12009
- Vieira, E. M. F., Pires, A. L., Silva, J. P. B., Magalhães, V. H., Grilo, J., Brito, F. P., Silva, M. F., Pereira, A. M., & Goncalves, L. M. (2019). High-Performance μ-Thermoelectric Device Based on Bi2Te3/Sb2Te3 p-n Junctions. *ACS Applied Materials and Interfaces*, 11(42), 38946–38954. https://doi.org/10.1021/acsami.9b13254
- Wanarattikan, P., Jitthammapirom, P., Sakdanuphab, R., & Sakulkalavek, A. (2019a). Effect of Grain Size and Film Thickness on the Thermoelectric Properties of Flexible Sb2Te3 Thin Films. *Advances in Materials Science and Engineering*, 2019. https://doi.org/10.1155/2019/6954918
- Wanarattikan, P., Jitthammapirom, P., Sakdanuphab, R., & Sakulkalavek, A. (2019b). Effect of Grain Size and Film Thickness on the Thermoelectric Properties of Flexible Sb2Te3 Thin Films. *Advances in Materials Science and Engineering*, 2019. https://doi.org/10.1155/2019/6954918
- Witting, I. T., Chasapis, T. C., Ricci, F., Peters, M., Heinz, N. A., Hautier, G., & Snyder, G. J. (2019). The Thermoelectric Properties of Bismuth Telluride. In *Advanced Electronic Materials* (Vol. 5, Issue 6). Blackwell Publishing Ltd. https://doi.org/10.1002/aelm.201800904
- Witting, I. T., Ricci, F., Chasapis, T. C., Hautier, G., & Snyder, G. J. (2020). The Thermoelectric Properties of n-Type Bismuth Telluride: Bismuth Selenide Alloys Bi2Te3-xSex. *Research*, 2020. https://doi.org/10.34133/2020/4361703

- Xu, H., Zhang, Q., Yi, L., Huang, S., Yang, H., Li, Y., Guo, Z., Hu, H., Sun, P., Tan, X., Liu, G., Song, K., & Jiang, J. (2022). High performance of Bi2Te3-based thermoelectric generator owing to pressure in fabrication process. *Applied Energy*, 326, 119959. https://doi.org/10.1016/j.apenergy.2022.119959
- Yang, X., Wang, C., Lu, R., Shen, Y., Zhao, H., Li, J., Li, R., Zhang, L., Chen, H., Zhang, T., & Zheng, X. (2022).
 Progress in measurement of thermoelectric properties of micro/nano thermoelectric materials: A critical review. In *Nano Energy* (Vol. 101). Elsevier Ltd. https://doi.org/10.1016/j.nanoen.2022.107553
- Yonezawa, S., Tabuchi, T., & Takashiri, M. (2020). Atomic composition changes in bismuth telluride thin films by thermal annealing and estimation of their thermoelectric properties using experimental analyses and firstprinciples calculations. *Journal of Alloys and Compounds*, 841. https://doi.org/10.1016/j.jallcom.2020.155697
- Zang, J., Ma, Y., Zhao, Y., Guo, R., Liu, Y., Liu, D., & Xue, C. (2023). Effect of post-annealing treatment on the thermoelectric properties of Ag2Se flexible thin film prepared by magnetron sputtering method. *Results in Physics*, 45. https://doi.org/10.1016/j.rinp.2023.106222
- Zeng, Y. J., Wu, D., Cao, X. H., Zhou, W. X., Tang, L. M., & Chen, K. Q. (2020). Nanoscale Organic Thermoelectric Materials: Measurement, Theoretical Models, and Optimization Strategies. In *Advanced Functional Materials* (Vol. 30, Issue 8). Wiley-VCH Verlag. https://doi.org/10.1002/adfm.201903873
- Zhang, X., Sun, Y., Wang, M., Cui, H., Xie, W., Shen, L., & Guo, W. (2019). Facilitating electron collection of organic photovoltaics by passivating trap states and tailoring work function. Solar Energy, 181, 9–16. https://doi.org/10.1016/j.solener.2019.01.077
- Zhao, Y., Li, L., Lu, Z., Teng, G., Liu, S., Hu, Z., & He, A. (2021). The effect of annealing temperature on the recrystallization and mechanical properties of severe plastic deformed commercial pure aluminium during ultra-fast annealing. *Materials Research Express*, 8(4). https://doi.org/10.1088/2053-1591/abf3e3
- Zheng, Y., Song, W., Song, Z., Zhang, Y., Xin, T., Liu, C., Xue, Y., Song, S., Liu, B., Lin, X., Kuznetsov, V. G., Tupitsyn, I. I., Kolobov, A. V., & Cheng, Y. (2024). A Complicated Route from Disorder to Order in Antimony–Tellurium Binary Phase Change Materials. Advanced Science, 11(9). https://doi.org/10.1002/advs.202301021
- Zheng, Z. hao, Yang, D., Zhang, P. cheng, Li, F., Chen, Y. xing, Liang, G. xing, & Fan, P. (2020). Enhancement of the thermoelectric properties of Bi2Te3 nanocrystal thin films by rapid annealing. *Materials Letters*, 275. https://doi.org/10.1016/j.matlet.2020.128143
- Zhu, Q., Wang, S., Wang, X., Suwardi, A., Chua, M. H., Soo, X. Y. D., & Xu, J. (2021). Bottom-Up Engineering Strategies for High-Performance Thermoelectric Materials. In *Nano-Micro Letters* (Vol. 13, Issue 1). Springer Science and Business Media B.V. https://doi.org/10.1007/s40820-021-00637-z